Hindawi Publishing Corporation
Advances in Materials Science and Engineering
Volume 2016, Article ID 2914368, 8 pages
http://dx.doi.org/10.1155/2016/2914368

Research Article

Effects of Calcination on the Crystallography and Nonbiogenic Aragonite Formation of Ark Clam Shell under Ambient Condition

Chee Wah Loy,[1,2] Khamirul Amin Matori,[1,3] Way Foong Lim,[3] Siegbert Schmid,[2] Norhazlin Zainuddin,[4] Zaidan Abdul Wahab,[1] Zarifah Nadakkavil Alassan,[1] and Mohd Hafiz Mohd Zaid[1]

[1]*Department of Physics, Faculty of Science, Universiti Putra Malaysia (UPM), 43400 Serdang, Selangor, Malaysia*
[2]*School of Chemistry, The University of Sydney, F11, Eastern Avenue, Sydney, NSW 2006, Australia*
[3]*Materials Synthesis and Characterization Laboratory, Institute of Advanced Technology, Universiti Putra Malaysia (UPM), 43400 Serdang, Selangor, Malaysia*
[4]*Department of Chemistry, Faculty of Science, Universiti Putra Malaysia (UPM), 43400 Serdang, Selangor, Malaysia*

Correspondence should be addressed to Khamirul Amin Matori; khamirul@upm.edu.my

Received 18 November 2015; Accepted 11 January 2016

Academic Editor: Michele Iafisco

This paper presents a study of crystallographic evolution of disposed ark clam shell (ACS) after calcination at 400–1400°C which was kept at room temperature under ambient condition in Malaysia during nine months. A better understanding of hydration and recarbonation of ACS powder (≤63 μm) after calcination was discovered by PXRD and FTIR. The research focuses on the crystallographic transformation, biogenic calcite decomposition, and unusual atmospheric aragonite formation in ACS after calcination and atmospheric air exposure. Ex situ PXRD showed calcite present in ACS at ≤900°C. ACS transformed to pyrogenic fcc CaO at ≥800°C after three months. Long term atmospheric air exposure of decarbonized ACS caused nucleation of nonbiogenic aragonite, vaterite, calcite, and portlandite. However, in situ PXRD analysis of ACS at instantaneous temperature without cooling process does not indicate the presence of aragonite, vaterite, and portlandite crystals. FTIR spectra revealed CaO–CO_2 bond in ACS dissociated with temperature (600–900°C) to form CaO and CO_2. Ca–OH bond was also traced in FTIR spectra of ≥700°C. It resulted by hydroadsorption of CaO with H_2O in atmospheric air.

1. Introduction

There are many aquatic organisms such as bivalve seashells which consist of exoskeleton which is made by biomineralization of calcium carbonate ($CaCO_3$). Many species of bivalve seashells are our seafood. Their shells may consist of naturally formed biogenic $CaCO_3$ which exist in several crystallographic polymorphs such as calcite (R-trigonal), aragonite (P-orthorhombic), and vaterite (P-hexagonal) [1, 2]. The difference in the crystalline phases precipitated during biomineralization depends on the nucleation barrier, pH, temperature, and concentrations of some inorganic mineral ions in sea water [3, 4]. In general, most clam shells (e.g., *Anadara granosa*) and oyster shells (e.g., *Crassostrea gigas*) consist of biogenic calcite [5–7], whereas mussels [7], *Acanthocardia tuberculata* [8], *Unio terminalis* [9], *Nautilus macromphalus* [9], and abalone shells [10] consist of biogenic aragonite.

In nature, aragonite formed by geogenic process under high pressure at low temperature or biogenic process [11]. Besides, $CaCO_3$ also exists naturally in three pseudopolymorphs of hydrated $CaCO_3$. They are amorphous $CaCO_3{\cdot}xH_2O$ ($x \approx 1$), P-hexagonal $CaCO_3{\cdot}H_2O$ (monohydrocalcite), and C-monoclinic $CaCO_3{\cdot}6H_2O$ (ikaite) crystals [12–15]. The species of ark clam is being chosen for our research because it solely consists of biogenic calcite and is the most consumed seafood bivalve in Malaysia and most countries. It is categorized under the kingdom of Animalia, phylum of Mollusca, class of Bivalvia, subclass of

Pteriomorphia, order of Arcoida, family of Arcidae, genus of *Anadara*, and species of *granosa* [16]. The shells of ark clam (ACS) contribute large amount of solid waste. ACS is primarily composed of $CaCO_3$ which is mostly in the form of calcite. When sufficient heat is applied to calcite, it will decompose to form calcium oxide (CaO) and release carbon dioxide (CO_2) gas.

In this study, we reported crystallographic evolution and unusual nonbiogenic aragonite formation of disposed ACS powder after calcination at 400–1400°C for 3 hours followed by slow cooling rate (−10°C min^{-1}) under moist atmospheric air and pressure in Malaysia which has not been reported by other researchers. Disposed ACS was used as a source of high crystallinity biogenic calcite. Utilization of ACS and other seafood shells can reduce lands for mining limestone and reduce solid waste associated with seafood industries. Partial pressures of carbon dioxide in atmospheric air affect the recarbonation of decarbonized ACS, whereas partial pressure of water vapour in atmospheric air affects hydroadsorption of hygroscopic CaO during cooling process. The ambient condition also caused recarbonation of pyrogenic fcc CaO to form atmospheric aragonite and atmospheric calcite by CO_2-chemoadsorption. The formation of aragonite from CaO under ambient condition is unusual because it is thermodynamically less stable compared to calcite. It was first discovered by Loy (2012) and further discussed in this paper. PXRD and FTIR analyses were carried out to describe the decomposition of calcite, formation of aragonite, and hydroadsorption of CaO in terms of crystallography and chemical bonds change of ACS [17].

2. Materials and Methods

The raw material of this study was fresh disposed ACS by seafood industries in West Peninsular Malaysia. The ACS originates from Straits of Malacca. ACS was immersed into bleaching detergent (0.5–2% of sodium hypochlorite, NaClO) for 30 minutes and then rinsed with water. NaClO was practically used by other researchers before to remove organic compounds on calcium-based materials such as aragonite, hydroxyapatite, and bone [18–20]. Clean ACS was ground into powder (≤63 μm) and tested by PXRD under wide range of angles (10–130°) to identify the purity of crystals.

Clean ACS was also heated at 400°C for 3 hours to be brittle, easy to grind, and free of organic compounds. The ACS was ground into powder (≤63 μm) for in situ PXRD analysis under ambient condition. In situ PXRD analysis was performed by PANalytical X'Pert Pro PW3050/60 diffractometer with CuK_α radiation and stage furnace to characterize ACS powder while being heated at 600–1000°C under ambient condition. The decomposition temperature and phase transformation of calcite under ambient condition were determined.

In order to study the effect of atmospheric air in Malaysia on ACS after calcination, ACS powder was calcined at various temperatures (400–1400°C) for 3 hours in an electric furnace under ambient condition. Each calcined ACS powder was heated with a rate of +10°C min^{-1}, remained at calcination temperature for 3 hours, and then cooled with a rate of −10°C min^{-1} to room temperature. The products of calcination were reground into powder (≤63 μm) and kept for three and nine months for further analyses. Ex situ PXRD test was also carried out by PANalytical X'Pert Pro PW3050/60 diffractometer with CuK_α radiation at room temperature to characterize calcined ACS powder. The scanning angles (2θ) of ex situ PXRD were 10–70°. The decomposition temperature and phase transformation of calcite under ambient condition were determined. The result was compared to the in situ PXRD patterns of ACS after calcination under ambient condition.

FTIR spectroscopy was performed by PerkinElmer Spectrum 100 Series with universal attenuated total reflectance (UATR) technique to identify the chemical bonds existing in the calcined ACS powder after three months. The wave number range of IR spectra was 4000–280 cm^{-1}. The infrared (IR) absorption of calcite is contributed by three intramolecular (ν_3 = 1484, ν_4 = 706, and ν_2 = 885 cm^{-1}), three translator lattice (357, 330, and 182 cm^{-1}), and two rotator lattice vibrations (106 cm^{-1}) [21, 22]. Farmer (1974) stated that the three intramolecular modes are strongly polarized bands in the mid-IR, whereas the other five are in the far-IR [23]. Reig et al. (2002) used constant ratio method in the FTIR quantitative analysis of calcite. They found the IR absorption bands of calcite at 1420, 875, and 712 cm^{-1} [2]. Presence of aragonite can be identified obviously from IR absorption band of symmetric stretch vibration ν_1 which is IR-active. According to Bhagavantam and Venkatarayudu (1939), the IR bands of aragonite are positioned at ν_3 = 1504, 1492; ν_1 = 1080; ν_4 = 711, 706; and ν_2 = 866 cm^{-1}, whereas those of calcite are positioned at ν_3 = 1429–1492; ν_4 = 706; and ν_2 = 879 cm^{-1} [24]. Farmer (1974) showed the FTIR spectrum of CaO with impurities of $Ca(OH)_2$ and $CaCO_3$ [23]. The spectrum consists of a broad band at 700–200 cm^{-1} (overlapping of CaO and $CaCO_3$ absorption) and a sharp band at ~3600 cm^{-1} ($Ca(OH)_2$ absorption).

Chen and Xiang (2009) studied the three polymorphs of synthetic $Ca(CO)_3$ through displacement reaction of salt solutions ($CaCl_2$ and NH_4HCO_3) at 30–80°C [1]. They provided PXRD pattern and FTIR spectra to show crystals transformation of vaterite and calcite to aragonite. They stated that ν_2 and ν_4 vibrations of CO_3^{2-} bonds in vaterite are 877 and 744 cm^{-1}, respectively, whereas the vibrations of calcite bonds are 848 and 714 cm^{-1}, respectively. The IR absorption at ν_2 = 854, ν_4 = 712, and ν_4 = 700 cm^{-1} corresponds to the vibrations of CO_3^{2-} bonds in aragonite.

Ruiz et al. (2009) characterized $Ca(CO)_3$, CaO, and $Ca(OH)_2$ from lime for constructive application through PXRD and FTIR [25]. The IR absorption of $CaCO_3$ is positioned at 2875 (C=O bond), 1795 (C=O bond), 1444 (C–O bond), 877 (C–O bond), and 474 cm^{-1} (Ca–O). Two strong bands at 1444 and 877 cm^{-1} as well as a weak band at 713 cm^{-1} correspond to elongation modes of Ca–O bond of calcite. Mid-IR ranges of both CaO and $Ca(OH)_2$ spectra are almost similar. Presence of CaO was indicated by IR absorption bands at 3643, 1417, 866, and 511 cm^{-1}, whereas presence of $Ca(OH)_2$ was indicated by IR absorption bands at 3643, 2513, 1427, 1126, 875, and 457 cm^{-1}. However, less

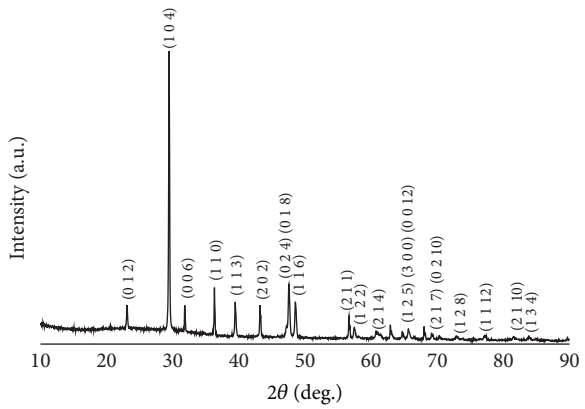

Figure 1: PXRD pattern of fresh ACS before calcination, where (h, k, l) are Miller indices of peaks attributed to R-trigonal $CaCO_3$ crystal.

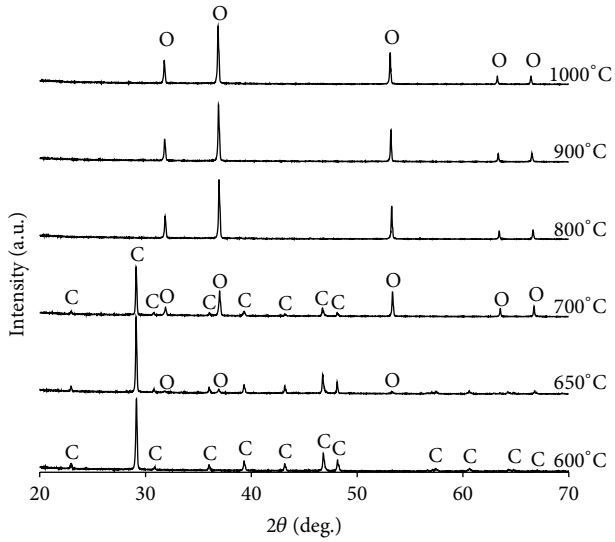

Figure 2: In situ PXRD patterns of ACS when calcined at 600–1000°C under ambient condition (C = calcite; and O = fcc CaO).

hydrated CaO has a weaker band at 3643 cm^{-1} compared to $Ca(OH)_2$.

3. Result and Discussion

PXRD test on ACS before calcination revealed that ACS consists of high crystallinity of R-trigonal $CaCO_3$ (biogenic calcite). No impure crystal was traced in the PXRD result in $10^\circ < 2\theta < 130^\circ$. Figure 1 shows the PXRD result in diffraction angle range of 10–90° which consists of most informative peaks which corresponded to calcite. These peaks are located at 2θ (Miller indices) = 23.12° (0 1 2), 29.46° (1 0 4), 31.84° (0 0 6), 36.33° (1 1 0), 39.45° (1 1 3), 43.19° (2 0 2), 47.56° (0 1 8)(0 2 4), 48.53° (1 1 6), 56.63° (2 1 1), 57.43° (1 2 2), 60.71° (2 1 4), 62.89° (1 2 5), 64.70° (3 0 0), 65.62° (0 0 12), 69.21° (2 1 7), 70.32° (0 2 10), 72.96° (1 2 8), 77.22° (1 1 12), 81.58° (2 1 0), and 83.88° (1 3 4). They were well matched with the ICSD 073446.

In situ PXRD scanning was also carried out on ACS heated from room temperature to 1000°C in a PXRD instrument installed with a stage furnace accessory. Crystallographic evolution of ACS at instantaneous temperature under atmospheric air and pressure was investigated. The in situ PXRD result of ACS at 600–1000°C is shown in Figure 2. It revealed that biogenic calcite in ACS powder slightly grows at 600–650°C. $CaCO_3$ began to decompose to fcc CaO at 650°C. Three major peaks of fcc CaO were found in the PXRD pattern at 31.79°, 36.93°, and 53.28°. Calcite in ACS does not transform into other polymorphs of $CaCO_3$ before decomposition. Calcite fully decomposed to form fcc CaO at 800°C. The fcc CaO only slightly grows towards 1000°C.

Figure 3 shows the ex situ PXRD patterns of ACS powder after calcination at 600–1000°C for 3 hours and cooling down to room temperature with a rate of −10°C min^{-1} under ambient condition. The PXRD pattern of ACS after calcination at 600°C showed a set of peaks attributed to calcite. Few major peaks of fcc CaO observed in the PXRD pattern of 700°C revealed that the biogenic calcite began to be decarbonized to form pyrogenic fcc CaO nucleate [5, 26, 27]. Calcite peaks intensity was diminished in the PXRD patterns

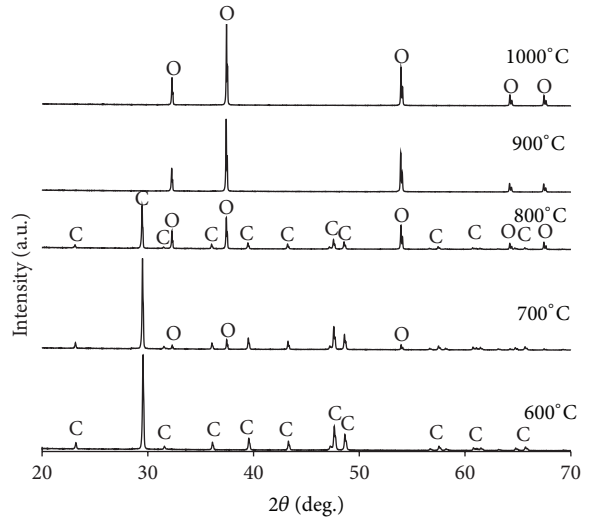

Figure 3: PXRD patterns of ACS after calcination at 600–1000°C for 3 hours and cooling down with −10°C min^{-1} under ambient condition (C = calcite; O = fcc CaO).

of 700–800°C and fully disappeared in the PXRD patterns of 900–1000°C. Full set of fcc CaO peaks was observed in the PXRD patterns of 800–1000°C. The increment of the fcc CaO peaks intensity in the patterns of 700–1000°C revealed that the crystal was growing in the temperature range. The pyrogenic fcc CaO peaks in the pattern of 1000°C were positioned at 2θ (Miller indices) = 32.29° (1 1 1), 37.45° (2 0 0), 53.95° (2 2 0), 64.24° (3 1 1), and 67.47° (2 2 2) sharply.

Figure 4 shows the ex situ PXRD patterns of ACS powder after calcination at 400–1400°C which were kept at room temperature under ambient condition for three months. The main objective of this analysis is to observe time-dependent crystallography evolution of ACS due to recarbonation and hydroadsorption of pyrogenic fcc CaO. The identities of

Table 1: Several crystal structures of calcium compounds present in ACS after calcination and kept under ambient condition for three months.

Mineral name	Calcite	Aragonite	Vaterite	Portlandite	Lime
Molecular formula	$CaCO_3$	$CaCO_3$	$CaCO_3$	$Ca(OH)_2$	CaO
ICSD code	073446	032100	18127	202231	75785
Crystal system	Trigonal	Orthorhombic	Hexagonal	Trigonal	Cubic
Bravais lattice	Rhombohedral	Primitive	Primitive	Primitive	Face-centered
Space group	D^6_{3d} ($R\bar{3}c$)	D^{16}_{2h} (Pmcn)	D^4_{6h} ($P6_3/mmc$)	D^3_{3d} ($P\bar{3}m1$)	O^4_h ($Fm\bar{3}m$)
a (nm)	0.4991	0.49610	7.135	0.36041	0.48106
b (nm)	0.4991	0.79670	7.135	0.36041	0.48106
c (nm)	1.7062	0.57410	16.98	0.49620	0.48106

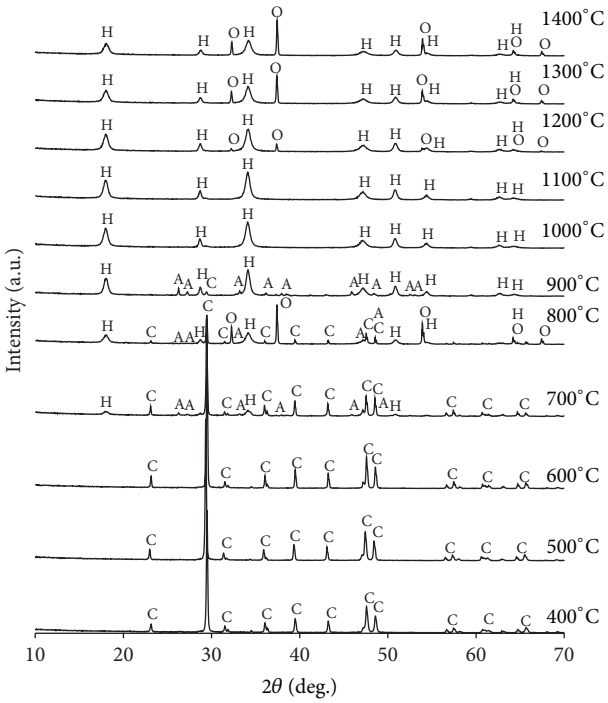

Figure 4: PXRD patterns of ACS after calcination at 400–1400°C for 3 hours and cooling down with −10°C min^{-1}, which were kept under ambient condition for three months (C = calcite; A = aragonite; H = P-trigonal $Ca(OH)_2$; and O = fcc CaO).

crystals found in the ex situ PXRD patterns are listed in Table 1. Biogenic calcite phase remains in the patterns of 400–800°C. The calcite peaks in the PXRD pattern of 600°C were matched with ICSD 073446 of calcite. No peak attributed to impure crystal was found. Sharp peaks of calcite are positioned at 2θ (Miller indices) = 23.14° (0 1 2), 29.49° (1 0 4), 31.51° (0 0 6), 36.05° (1 1 0), 39.47° (1 1 3), 43.22° (2 0 2), 47.15° (0 2 4), 47.56° (0 1 8), 48.57° (1 1 6), 56.65° (2 1 1), 57.45° (1 2 2), 58.16° (1 0 10), 60.74° (2 1 4), 61.48° (1 1 9), 62.98° (1 2 5), 64.71° (3 0 0), and 65.65° (0 0 12). The result matched with the PXRD pattern shown in Nave et al. (2004) [28].

The ex situ PXRD patterns of 700–900°C showed peaks attributed to calcite, P-orthorhombic $CaCO_3$ (aragonite), and P-trigonal $Ca(OH)_2$ (portlandite). Peaks attributed to portlandite are positioned at 2θ = 17.96° (0 0 1), 28.72° (1 0 0), 34.08° (1 0 1), 47.13° (1 0 2), and 50.83° (1 1 0). $Ca(OH)_2$ was formed by spontaneous reaction of pyrogenic CaO slaked with moisture content in atmospheric air during long period of cooling process and air exposure [25]. The nucleation and growing of portlandite crystal started to occur since the pyrogenic CaO has been cooled down slowly from dehydration temperature of $Ca(OH)_2$ (~600°C) to room temperature. Therefore, portlandite was not found in the in situ PXRD pattern of ACS heating at instantaneous temperatures (≥700°C) under ambient condition (Figure 2). $Ca(OH)_2$ can be dehydrated to form CaO by reheating it at 350–600°C under anhydrous condition [29, 30]. Besides P portlandite, PXRD patterns at 700–900°C also showed the presence of aragonite. Aragonite was traceable at 2θ (Miller indices) = 26.28° (1 1 1), 27.26° (0 2 1), 33.15° (0 1 2), 37.92° (1 1 2), 45.91° (2 2 1), and 48.52° (2 0 2). These peaks were well matched with ICSD 032100 of aragonite. Since aragonite is thermodynamically unstable compared to calcite, transformation of calcite to aragonite at high temperature under ambient condition is impossible [31, 32]. Several paths were taken by ACS to form atmospheric aragonite. First, biogenic calcite was decarbonized to form pyrogenic fcc CaO at 700–900°C as shown in Figure 3. During the slow cooling process, some of CaO slaked with water from air to form P-trigonal $Ca(OH)_2$. Both CaO and $Ca(OH)_2$ also experienced recarbonation to form atmospheric $CaCO_3$ in order to reestablish dynamic equilibrium with CO_2 at room temperature under ambient condition [33]. Finally, $CaCO_3$ particles were realigned to form aragonite. The peaks intensity attributed to fcc CaO in the PXRD patterns of 700–900°C in Figure 3 diminished compared to the PXRD patterns at the same temperatures in Figure 4, revealing that fcc CaO was transformed to both $Ca(OH)_2$ and $CaCO_3$.

The recarbonation process of fcc CaO to $CaCO_3$ in air may involve two steps of phase transformation (fcc CaO to aragonite and aragonite to calcite). According to Ostwald's Step Rule, nonordered $CaCO_3$ particles could transform into unstable transient state such as vaterite and aragonite before transforming to the most thermodynamically stable state of calcite [3, 34, 35]. The atmospheric aragonite may be nucleated due to slow cooling process of ACS from calcite-aragonite transition temperature to room temperature and then further growing under ambient condition. The calcite peaks in PXRD patterns of 700–800°C (Figure 4) may be attributed to the diffraction of both biogenic and atmospheric

calcite. The formation of atmospheric calcite was significantly traced in PXRD pattern of 900°C (Figure 4), where few major peaks of calcite appearing at 29.44°, 36.16°, 39.50°, 42.16°, and 48.42° are not found in the PXRD pattern in Figure 3.

The presence of portlandite was shown in the PXRD patterns of the temperature around 1000–1400°C (Figure 4). It revealed that fcc CaO is very hydroscopic to adsorb water molecules from atmospheric air to form portlandite in three months. As a result, fcc CaO was not significantly traced in the PXRD patterns of 700–1100°C. Portlandite has the highest diffraction intensity in the pattern of 1100°C. Its peaks are positioned at 2θ (Miller indices) = 17.96° (0 0 1), 28.64° (1 0 0), 34.09° (0 1 1), 47.11° (0 1 2), 50.86° (1 1 0), 54.35° (1 1 1), 59.40° (2 0 0), 62.56° (2 0 1), and 64.28° (1 1 2). They matched with ICSD 202231 and the PXRD pattern shown in Ruiz et al. (2009) [25]. The PXRD patterns of 1000–1400°C do not show any peak attributed to atmospheric calcite and atmospheric aragonite. It revealed that high temperature of calcination process may improve the crystallinity of pyrogenic fcc CaO and can retain its structure from complete hydration by atmospheric air in three months. The hydrated form of pyrogenic fcc CaO which crystallized to portlandite crystal has higher chemical resistivity against recarbonation by atmospheric air. The highest peaks intensity of fcc CaO was found in the PXRD pattern of 1400°C. They are positioned at 2θ (Miller indices) = 32.30° (1 1 1), 37.44° (1 1 1), 53.92° (2 2 0), 64.21° (3 1 1), and 67.44° (2 2 2). The result was well matched with ICSD 75785 and the PXRD pattern shown in Nave et al. (2004) [28].

Figure 5 showed FTIR spectra of ACS after calcination at 400–1400°C which were kept at room temperature under ambient condition for three months. ACS which has been calcined at 400°C has three strong IR absorption bands at 1399, 870, and 711 cm^{-1}. These bands indicated the presence of $CO_3{}^2$ attached to calcium ion (Ca^{2+}) in calcite structure [2, 5, 22, 25]. These bands also correspond to the modes of asymmetric stretch (ν_4), out-plane bend (ν_2), and in-plane bend (ν_3) vibrations of C–O bonds in calcite [21, 23, 24, 36]. A weak IR absorption band at 1793 cm^{-1} corresponded to C=O bond in calcite [25]. Besides, three weak IR absorption bands were found in the spectrum at 3743 and 2512 cm^{-1}. They were attributed to bond vibration of H–OH of water and Ca–OH_2 of calcite. We deduced that H_2O from atmospheric air was adsorbed by $CaCO_3$ via chemisorption and physisorption. Chemisorption of H_2O may form tiny hydrated $CaCO_3$ crystal which is below the detectable range of PXRD. Monohydrocalcite crystal is more likely to be presented in ACS compared to amorphous $CaCO_3$ and ikaite because monohydrocalcite is more kinetically stable at room temperature and pressure [13, 37, 38]. The chemical equation which represents the hydroadsorption of calcite was shown in (1). The FTIR spectra of ACS after calcination from 400 to 600°C do not show any significant changes in chemical bonds:

$$\mathrm{CaCO_3\ (s, biogenic\ calcite) + } x\mathrm{H_2O\,(g) \longrightarrow CaCO_3 \cdot } x\mathrm{H_2O\ (s, monohydrocalcite)} \tag{1}$$

FTIR spectrum changed as ACS was being calcined at 700°C. Two new IR absorption bands appeared at 3640 and 502 cm^{-1} in the FTIR spectrum of 700°C. They were contributed by vibration of Ca–OH bond in $Ca(OH)_2$ and Ca–O bond in CaO [36]. The strong and sharp band at 1408 cm^{-1} was resultant IR absorptions by asymmetric C–O bond vibration in calcite/aragonite and Ca–O bond vibration in CaO [25]. The spectrum revealed that biogenic $CaCO_3$ was partially decomposed to form pyrogenic CaO during calcination (see (2)) and then hydrated to form atmospheric $Ca(OH)_2$ under ambient condition (see (3)) [25, 39]. The result was consistent with the PXRD result of 700°C in Figure 4. The IR absorption bands of $CaCO_3$ in the spectrum may have resulted by the overlapping of IR absorption of biogenic calcite as well as recarbonized atmospheric calcite and aragonite (see (4)):

$$\mathrm{CaCO_3\ (s, biogenic\ calcite) \longrightarrow CaO\ (s, pyrogenic\ fcc) + CO_2\,(g)} \tag{2}$$

$$\mathrm{CaO\ (s, pyrogenic\ fcc) + H_2O\,(g) \longrightarrow Ca\,(OH)_2\ (s, atmospheric\ portlandite)} \tag{3}$$

$$\mathrm{CaO\ (s, pyrogenic\ fcc) + CO_2\,(g) \longrightarrow CaCO_3}\left(\mathrm{s, \frac{atmospheric\ aragonite}{calcite}}\right) \tag{4}$$

Ca^{2+} has high magnitude of charge and small ionic radius. Therefore, it has high charge density and polarization strength. $CO_3{}^{2-}$ in calcite has larger ionic size compared to O^{2-} in CaO. The large electron cloud of $CO_3{}^{2-}$ can be polarized by Ca^{2+} and ascended higher covalent character of CaO–CO_2 bond in calcite. At high temperature, Ca^{2+} pulls electron pair of Ca–OCO_2 closer towards itself and strengthens the bond. Large ionic size of $CO_3{}^{2-}$ caused the CaO–CO_2 bond to experience larger magnitude of bond strain of vibration. It weakens the CaO–CO_2 bond strength at high temperature. With calcination ≥700°C, calcite gained enough energy to break the CaO–CO_2 bond and form CaO and CO_2 gas as shown in (2). Ca–O bond in CaO has higher ionic character and higher bond strength than Ca–OCO_2 in

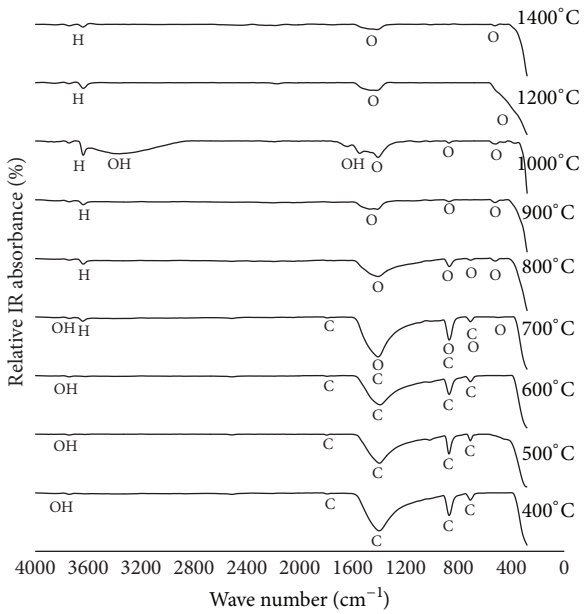

Figure 5: IR absorption spectra of ACS after calcination at 400–1400°C for 3 hours and cooling down with –10°C min^{-1}, which were kept under ambient condition for three months (C = bonds of calcite; OH = O–H and Ca–OH_2 bonds of water; H = Ca–OH in $Ca(OH)_2$; and O = Ca–O bond in CaO).

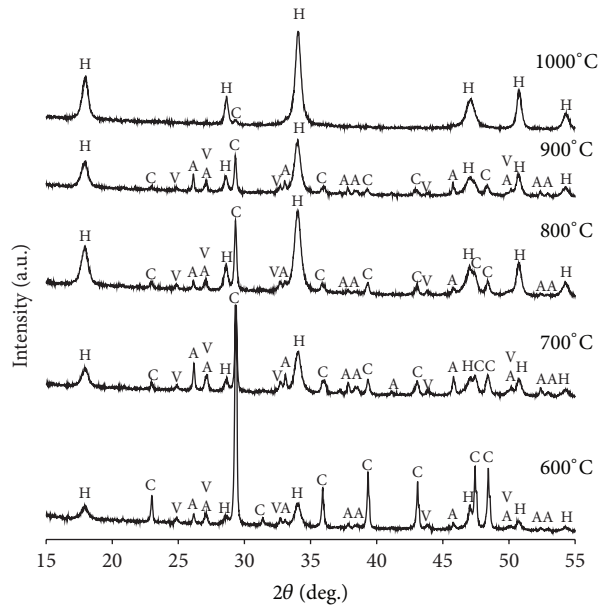

Figure 6: PXRD patterns of ACS after calcination at 600–1000°C for 3 hours and cooling down with –10°C min^{-1}, which were kept under ambient condition for nine months (C = calcite; A = aragonite; H = P-trigonal $Ca(OH)_2$; and O = fcc CaO).

calcite. Therefore, CaO has higher thermodynamic stability than calcite at high temperature.

CaO has higher hydroadsorption strength than calcite because it is more polar than calcite. Both Ca^{2+} and O^{2-} sites in CaO can undergo physisorption with H_2O to form Ca–OH_2 bond. Besides, large ionic size of $CO_3{}^{2-}$ in $CaCO_3$ reduced free site of Ca to adsorb H_2O. CaO also has high chemisorption strength with H_2O to form $Ca(OH)_2$ with Ca–OH bonds. $Ca(OH)_2$ is more kinetically stable than CaO because CaO has low activation energy to react with H_2O exothermically to form $Ca(OH)_2$ (see (3)). As a result, $Ca(OH)_2$ was traced in the FTIR spectrum of 700°C as CaO formed by decomposition of $CaCO_3$.

The IR absorption bands of calcite/aragonite decreased in the spectrum of 800°C and disappeared in the spectrum of 900°C. Four IR absorption bands in the FTIR spectra of 800°C positioned at 2190, 1415, 875, and 520 cm^{-1} were attributed to the presence of CaO [25]. The IR absorption bands of CaO increased from 700 to 1000°C. It revealed that the content of CaO increased. Since CaO has a hygroscopic property, the formation of $Ca(OH)_2$ increased parallel with the increases of CaO particles. It was supported by FTIR spectra which showed that IR absorption bands of $Ca(OH)_2$ increased from 700 to 1000°C. The highest hydroadsorption strength of ACS was achieved as it was cooled down from 1000°C. A new broad band at 3640–2800 cm^{-1} appeared in the FTIR spectrum of 1000°C. It represented the presence of Ca–OH_2 and H–OH bonds due to physisorption of water by CaO.

The FTIR spectra of 1200 and 1400°C showed that the IR absorption bands of CaO decreased. It was due to the fact that further crystallization of fcc CaO at higher temperature limited the magnitude of Ca–O bond vibrations. However, the intensity of IR band attributed to hydroxide ions (OH^-) at ~3640 cm^{-1} does not change significantly. It revealed that the high crystallinity of fcc CaO at high temperature limited the nucleation and growth of $Ca(OH)_2$ crystal (Figure 3). No IR absorption band attributed to calcite and aragonite was found in the spectra. Hence, we deduced that high crystallinity of fcc CaO can slow down the recarbonation rate of CaO.

In order to further investigate the time-dependent recarbonation and hydration of calcined ACS at 600–1000°C exposed to atmospheric air, PXRD tests were carried out after nine months of calcination and the result was shown in Figure 6. The results revealed that ACS samples underwent decarbonation, hydration, and recarbonation. The PXRD pattern of 600°C was matched with the diffraction patterns of calcite, aragonite, vaterite, and portlandite. The major phase was calcite. The result showed that the original biogenic calcite was decarbonized and hydrated by atmospheric air to form portlandite. Conversion of stable calcite phase to less stable aragonite and vaterite polymorphs under ambient temperature and pressure is not thermodynamically favourable crystallographic transformation. The crystallization of aragonite and vaterite reflects the fact that the original biogenic calcite in ACS was decarbonized and recarbonized by atmospheric air. The recarbonized $CaCO_3$ might form the least stable of amorphous $CaCO_3$ polymorphs first before recrystallization. The amorphous $CaCO_3$ underwent nucleation of vaterite first followed by transformation towards more stable aragonite and then the most stable calcite [35]. The presence of aragonite was observed at 2θ = 26.16°, 27.10°, 33.12°, 35.92°, 37.85°, 38.45°, 45.80°, 50.04°, 52.39°, and 52.95°,

whereas vaterite was observed at 2θ = 24.96°, 27.10°, 32.71°, 43.81°, 48.58°, and 50.04°. Hence, the diffraction of calcite observed in the pattern resulted by both biogenic calcite and atmospheric calcite. The crystallization of portlandite reflects the fact that the original biogenic calcite in ACS was decarbonized to CaO, hydrated to $Ca(OH)_2$, and then crystallized to form portlandite by atmospheric air. The presence of portlandite was observed at 2θ = 17.93°, 28.56°, 34.02°, 47.06°, 50.68°, and 54.25°.

The PXRD patterns of 700–900°C in Figure 6 also showed the presence of calcite, aragonite, vaterite, and portlandite. However, the patterns have lower diffraction intensity of calcite compared to the pattern of 600°C. It reflects the fact that the biogenic calcite in ACS was decarbonized to fcc CaO during calcination but does not fully recover by atmospheric recarbonation. The patterns do not show the presence of fcc CaO. It revealed that fcc CaO that crystallized during calcination is not stable when exposed to atmospheric air. In addition, CaO which decarbonized by atmospheric air does not crystallize to fcc CaO. The high hygroscopic behaviour of CaO made CaO adsorb water rapidly from atmospheric air to form portlandite and made it unable to retain its fcc CaO structure for long period. Besides, the pyrogenic fcc CaO also underwent recarbonation to form calcite, aragonite, and vaterite phases as shown in the patterns of 700–900°C. The sequence of hydration and recarbonation of CaO by atmospheric H_2O and CO_2 is expressed as follows:

$$CaO + CO_2 + H_2O \longleftrightarrow Ca(OH)_2 + CO_2 \longleftrightarrow CaCO_3 + H_2O \quad (5)$$

The PXRD pattern of 1000°C in Figure 6 only consists of diffraction pattern of portlandite and a main calcite peak at 29.32°. The result revealed that high crystallinity of pyrogenic fcc CaO which was exposed to atmospheric air formed a stable atmospheric portlandite phase. The portlandite phase has a high resistivity to inhibit recarbonation. Hence, small amount of atmospheric calcite was nucleated. No intermediate phase transition of $CaCO_3$ (aragonite and vaterite) was observed.

4. Conclusion

A series of calcinations at variation temperature (400–1400°C) was carried out on disposed ACS which originates from Straits of Malacca. In situ PXRD analysis was conducted on ACS powder at instantaneous temperatures under ambient condition, whereas ex situ PXRD analysis was conducted on ACS powder after calcination and cooling down ($-10°C\,min^{-1}$) to room temperature. In general, both in situ and ex situ PXRD analyses showed that the biogenic calcite in ACS is decarbonized to form pyrogenic fcc CaO at 650–800°C under ambient condition. The crystallinity of pyrogenic fcc CaO increases as calcination temperature increases. In situ PXRD result showed that the biogenic calcite grew at 600–650°C and is completely decarbonized at 800°C. The pyrogenic fcc CaO was nucleated at 650°C and further crystallized at higher temperature. However, ACS after decarbonation at ≥700°C and cooling down to room temperature under ambient condition induced reestablishment of new dynamic equilibrium via H_2O and CO_2 adsorption of pyrogenic CaO. Evidence of reestablishment of new dynamic equilibrium was observed from the PXRD analysis of decarbonized ACS after three months of atmospheric air exposure. Hydration of pyrogenic fcc CaO in atmospheric air induced crystallization of atmospheric portlandite in ACS after calcination at 700–1400°C. Recarbonation of pyrogenic fcc CaO in atmospheric air caused crystallization of atmospheric calcite as well as intermediate phase of aragonite and vaterite in the ACS after calcination at 700–900°C. The result agrees with Ostwald's Step Rule, where recarbonation of fcc CaO crystallizes the least stable polymorph of $CaCO_3$ first before transforming to stable calcite. The PXRD result also revealed that high crystallinity of pyrogenic fcc CaO has higher resistivity to recarbonation. fcc CaO is not a stable phase in atmospheric air. FTIR analysis on the ACS after calcination and three months of atmospheric air exposure under ambient condition reflects the hygroscopic effect on both calcite and CaO. Calcite slightly adsorbed H_2O to form monohydrocalcite in short range order. CaO is very hygroscopic. It adsorbed H_2O spontaneously to form $Ca(OH)_2$. ACS has highest degree of H_2O adsorption as ACS after decarbonation at 1000°C. FTIR spectrum also revealed that calcite decomposed at 600–800°C. CaO and $Ca(OH)_2$ coexisted in the ACS after cooling down from 700–1400°C to room temperature. Overall, PXRD analysis is more appropriate to study polymorphic transformation in recarbonation of pyrogenic CaO, whereas FTIR analysis is more appropriate to study hydration of biogenic calcite and pyrogenic CaO.

Conflict of Interests

The authors declare that there is no conflict of interests regarding the publication of this paper.

Acknowledgment

The authors gratefully acknowledge the financial support from the Malaysian Ministry of Higher Education (MOHE) through Research University Grant Scheme (RUGS).

References

[1] J. Chen and L. Xiang, "Controllable synthesis of calcium carbonate polymorphs at different temperatures," *Powder Technology*, vol. 189, no. 1, pp. 64–69, 2009.

[2] F. B. Reig, J. V. G. Adelantado, and M. C. M. Moya Moreno, "FTIR quantitative analysis of calcium carbonate (calcite) and silica (quartz) mixtures using the constant ratio method. Application to geological samples," *Talanta*, vol. 58, no. 4, pp. 811–821, 2002.

[3] W. Sun, S. Jayaraman, W. Chen, K. A. Persson, and G. Ceder, "Nucleation of metastable aragonite $CaCO_3$ in seawater," *Proceedings of the National Academy of Sciences of the United States of America*, vol. 112, no. 11, pp. 3199–3204, 2015.

[4] H. Nebel and M. Epple, "Continuous preparation of calcite, aragonite and vaterite, and of magnesium-substituted amorphous calcium carbonate (Mg-ACC)," *Zeitschrift fur Anorganische und Allgemeine Chemie*, vol. 634, no. 8, pp. 1439–1443, 2008.

[5] S. W. Lee, Y. M. Kim, R. H. Kim, and C. S. Choi, "Nanostructured biogenic calcite: a thermal and chemical approach to folia in oyster shell," *Micron*, vol. 39, no. 4, pp. 380–386, 2008.

[6] Y. S. Ok, S.-E. Oh, M. Ahmad et al., "Effects of natural and calcined oyster shells on Cd and Pb immobilization in contaminated soils," *Environmental Earth Sciences*, vol. 61, no. 6, pp. 1301–1308, 2010.

[7] F. Wheaton, "Review of oyster shell properties: part II. Thermal properties," *Aquacultural Engineering*, vol. 37, no. 1, pp. 14–23, 2007.

[8] B. Pokroy, J. P. Quintana, E. N. Caspi, A. Berner, and E. Zolotoyabko, "Anisotropic lattice distortions in biogenic aragonite," *Nature Materials*, vol. 3, no. 12, pp. 900–902, 2004.

[9] B. Pokroy, A. N. Fitch, and E. Zolotoyabko, "Structure of biogenic aragonite (CaCO3)," *Crystal Growth & Design*, vol. 7, no. 9, pp. 1580–1583, 2007.

[10] J. Wang, Y. Xu, Y. Zhao et al., "Morphology and crystalline characterization of abalone shell and mimetic mineralization," *Journal of Crystal Growth*, vol. 252, no. 1–3, pp. 367–371, 2003.

[11] G. Simmons and P. Bell, "Calcite-aragonite equilibrium," *Science*, vol. 139, no. 3560, pp. 1197–1198, 1963.

[12] L. Brečević and D. Kralj, "On calcium carbonates: from fundamental research to application," *Croatica Chemica Acta*, vol. 80, no. 3-4, pp. 467–484, 2007.

[13] B. Dickens and W. E. Brown, "The crystal structure of calcium carbonate hexahydrate at ~–120°," *Inorganic Chemistry*, vol. 9, no. 3, pp. 480–486, 1970.

[14] H. Nebel, M. Neumann, C. Mayer, and M. Epple, "On the structure of amorphous calcium carbonate—a detailed study by solid-state NMR spectroscopy," *Inorganic Chemistry*, vol. 47, no. 17, pp. 7874–7879, 2008.

[15] M. M. Tlili, M. B. Amor, C. Gabrielli, S. Joiret, G. Maurin, and P. Rousseau, "Characterization of $CACO_3$ hydrates by micro-Raman spectroscopy," *Journal of Raman Spectroscopy*, vol. 33, no. 1, pp. 10–16, 2002.

[16] M. J. Broom, "Gonad development and spawning in *Anadara granosa* (L.) (Bivalvia: Arcidae)," *Aquaculture*, vol. 30, no. 1–4, pp. 211–219, 1983.

[17] C. W. Loy, *Effects of heat treatment on structure and thermal diffusivites of SiO_2–Al_2O_3–Na_2O–CaO–CaF_2 glass-ceramics from waste materials [M.S. thesis]*, Universiti Putra Malaysia, 2012.

[18] J. D. Bronzino, "Tissue engineering and artificial organs," in *The Biomedical Engineering Handbook*, pp. 24–26, CRC Press, Boca Raton, Fla, USA, 3rd edition, 2006.

[19] S. Goffredo, P. Vergni, M. Reggi et al., "The skeletal organic matrix from Mediterranean coral *Balanophyllia europaea* influences calcium carbonate precipitation," *PLoS ONE*, vol. 6, no. 7, Article ID e22338, 7 pages, 2011.

[20] J. Mahamid, A. Sharir, L. Addadi, and S. Weiner, "Amorphous calcium phosphate is a major component of the forming fin bones of zebrafish: indications for an amorphous precursor phase," *Proceedings of the National Academy of Sciences of the United States of America*, vol. 105, no. 35, pp. 12748–12753, 2008.

[21] K. Nakamoto, *Infrared and Raman Spectra of Inorganic and Coordination Compounds, Part A: Theory and Applications in Inorganic Chemistry*, Wesley, New York, NY, USA, 6th edition, 1970.

[22] R. A. Nyquist and R. O. Kagel, *Infrared Spectra of Inorganic Compounds*, Academic Press, New York, NY, USA, 1971.

[23] V. C. Farmer, *The Infrared Spectra of Minerals*, Mineralogical Society, London, UK, 1974.

[24] S. Bhagavantam and T. Venkatarayudu, "Raman effect in relation to crystal structure," *Proceedings of the Indian Academy of Sciences A*, vol. 9, no. 3, pp. 224–258, 1939.

[25] M. G. Ruiz, J. Hernández, L. Baños, J. N. Montes, and M. E. R. García, "Characterization of calcium carbonate, calcium oxide, and calcium hydroxide as starting point to the improvement of lime for their use in construction," *Journal of Materials in Civil Engineering*, vol. 21, no. 11, pp. 694–698, 2009.

[26] H.-B. Kwon, C.-W. Lee, B.-S. Jun, J.-D. Yun, S.-Y. Weon, and B. Koopman, "Recycling waste oyster shells for eutrophication control," *Resources, Conservation and Recycling*, vol. 41, no. 1, pp. 75–82, 2004.

[27] N. Huang and J. Wang, "A TGA-FTIR study on the effect of $CaCO_3$ on the thermal degradation of EBA copolymer," *Journal of Analytical and Applied Pyrolysis*, vol. 84, no. 2, pp. 124–130, 2009.

[28] D. Nave, S. Rosenwaks, R. Vago, and I. Bar, "Pulsed laser deposition of marine origin material: preparation and characterization of $CaCO_3$ particles and CaO nanocrystals," *Journal of Applied Physics*, vol. 95, no. 12, pp. 8309–8313, 2004.

[29] J. O. Chae, S. P. Knak, A. N. Knak, H. J. Koo, and V. Ravi, "Oyster shell recycling and bone waste treatment using plasma pyrolysis," *Plasma Science and Technology*, vol. 8, no. 6, pp. 712–715, 2006.

[30] A. Irabien, J. R. Viguri, and I. Ortiz, "Thermal dehydration of calcium hydroxide. 1. Kinetic model and parameters," *Industrial & Engineering Chemistry Research*, vol. 29, no. 8, pp. 1599–1606, 1990.

[31] M. B. Toffolo and E. Boaretto, "Nucleation of aragonite upon carbonation of calcium oxide and calcium hydroxide at ambient temperatures and pressures: a new indicator of fire-related human activities," *Journal of Archaeological Science*, vol. 49, no. 1, pp. 237–248, 2014.

[32] G. Zhang, Y. Guo, J. Ao, J. Yang, G. Lv, and K. Shih, "Thermally induced phase transformation of pearl powder," *Materials Science and Engineering C*, vol. 33, no. 4, pp. 2046–2049, 2013.

[33] V. Morales-Flórez, A. Santos, I. Romero-Hermida, and L. Esquivias, "Hydration and carbonation reactions of calcium oxide by weathering: kinetics and changes in the nanostructure," *Chemical Engineering Journal*, vol. 265, pp. 194–200, 2015.

[34] S.-Y. Chung, Y.-M. Kim, J.-G. Kim, and Y.-J. Kim, "Multiphase transformation and Ostwald's rule of stages during crystallization ofametal phosphate," *Nature Physics*, vol. 5, no. 1, pp. 68–73, 2009.

[35] W. Ostwald, "Studien uber die bildung und umwandlung fester korper. 1. Abhandlung ubersattgung und uberkaltung," *Zeitschrift für Physikalische Chemie*, vol. 22, pp. 289–330, 1897.

[36] T. Witoon, "Characterization of calcium oxide derived from waste eggshell and its application as CO_2 sorbent," *Ceramics International*, vol. 37, no. 8, pp. 3291–3298, 2011.

[37] H. Hull and A. G. Turnbull, "A thermochemical study of monohydrocalcite," *Geochimica et Cosmochimica Acta*, vol. 37, no. 3, pp. 685–694, 1973.

[38] G. Marland, "The stability of $CaCO_3 \cdot 6H_2O$ (ikaite)," *Geochimica et Cosmochimica Acta*, vol. 39, no. 1, pp. 83–91, 1975.

[39] G. Vogg, L. J.-P. Meyer, C. Miesner, M. S. Brandt, and M. Stutzmann, "Polygermanosilyne calcium hydroxide intercalation compounds formed by topotactic transformation of $Ca(Si_{1-x}Ge_x)_2$ alloy zintl phases in ambient atmosphere," *Monatshefte für Chemie*, vol. 132, no. 10, pp. 1125–1135, 2001.